Trends in the Electrochemical Synthesis of H_2O_2

Enhancing Activity and Selectivity by Electrocatalytic Site Engineering

Verdaguer Casadevall, Arnau; Deiana, Davide; Karamad, Mohammadreza; Siahrostami, Samira; Malacrida, Paolo; Hansen, Thomas Willum; Rossmeisl, Jan; Chorkendorff, Ib; Stephens, Ifan

Published in:
International Nano Letters

Link to article, DOI:
10.1021/nl500037x

Publication date:
2014

Document Version
Publisher's PDF, also known as Version of record

NANO LETTERS

Letter

pubs.acs.org/NanoLett

Trends in the Electrochemical Synthesis of H_2O_2: Enhancing Activity and Selectivity by Electrocatalytic Site Engineering

Arnau Verdaguer-Casadevall,[†] Davide Deiana,[‡] Mohammadreza Karamad,[§] Samira Siahrostami,[§] Paolo Malacrida,[†] Thomas W. Hansen,[‡] Jan Rossmeisl,[§] Ib Chorkendorff,*[,†] and Ifan E. L. Stephens*[,†]

[†]Center for Individual Nanoparticle Functionality, Department of Physics, [‡]Center for Electron Nanoscopy, and [§]Center for Atomic-scale Materials Design, Department of Physics, Technical University of Denmark, DK-2800 Kongens Lyngby, Denmark

Supporting Information

ABSTRACT: The direct electrochemical synthesis of hydrogen peroxide is a promising alternative to currently used batch synthesis methods. Its industrial viability is dependent on the effective catalysis of the reduction of oxygen at the cathode. Herein, we study the factors controlling activity and selectivity for H_2O_2 production on metal surfaces. Using this approach, we discover two new catalysts for the reaction, Ag−Hg and Pd−Hg, with unique electrocatalytic properties both of which exhibit performance that far exceeds the current state-of-the art.

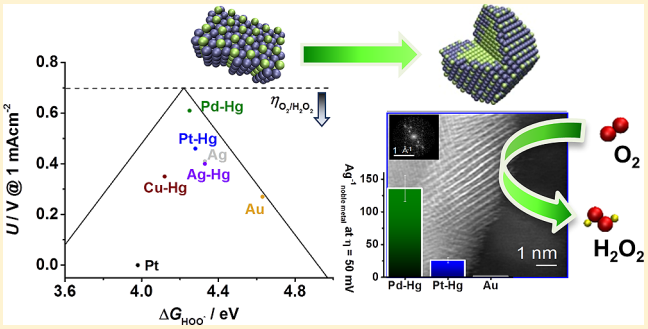

KEYWORDS: *H_2O_2 production, catalysis, electrochemistry, oxygen reduction, nanoparticles*

Economic development and a continued increase in global population place growing pressure on our energy resources. A significant fraction of the world's total energy consumption and raw materials are employed to produce chemicals. These chemicals are typically generated on a large scale in centralized locations.[1] However, localized chemical production, closer to the point of consumption, would present significant cost and energy savings. Electrochemical devices will play a major role in the transformation, as they can be operated at ambient temperatures and pressures in small plants and require minimal capital investment.[2]

Herein, we focus on the electrochemical oxygen reduction to hydrogen peroxide, a chemical whose electrochemical production is particularly appealing.[3] Currently, 3 M tons/year of H_2O_2 are being produced, mainly for use in the paper and chemical industry.[3] It is synthesized from hydrogen and oxygen by a complex batch method, the anthraquinone process, only suitable for large scale facilities.[4] The inherent disadvantages of batch synthesis methods and its energetic inefficiency have motivated industry and academia alike to develop an alternative. Consequently, the "direct catalytic" route to H_2O_2 synthesis has long been a dream reaction for the heterogeneous catalysis community; it involves the direct reaction of H_2 and O_2 in a liquid solvent on a Pd/Au catalyst.[5,6] Not only would the direct method enable production in a continuous mode, but it would also permit small scale, decentralized production. However, the direct route needs to handle potentially explosive mixtures of hydrogen and oxygen and does not make use of the embedded energy released upon reacting H_2.

A growing community of researchers are proposing an electrochemical route based on catalysts that selectively reduce oxygen to hydrogen peroxide.[7−9] That way, the danger of explosion is avoided by keeping hydrogen and oxygen separated. Moreover, producing H_2O_2 in a fuel cell would enable recovery of the energy released during the reaction. Alternatively, by producing it in an electrolyzer, one could avoid usage of H_2 altogether and use water as a source of protons.

Crucial to the performance of electrochemical devices for H_2O_2 production is the catalyst at the electrodes. A successful electrocatalyst should have (a) high activity, operating with high current densities as close as possible to the equilibrium potential, to optimize energy efficiency and catalyst loading; (b) high selectivity, ensuring high yields of H_2O_2; and (c) high stability, enabling long-term durability.

Significant efforts have been spent in the field of electrocatalysis to find descriptors for the trends in activity for electrochemical reactions. They all lead to a Sabatier volcano, where the highest activity is achieved on the surface with a moderate interaction with the reaction intermediates.[10−17] Most importantly, knowledge of this descriptor can lead to the discovery of new materials whose electrocatalytic performance exceeds the current state-of-the-art.[13,14,18,19]

The activity for H_2O_2 production is a function of the binding of the sole reaction intermediate, HOO* (Figure 1a).[20,21] For the ideal catalyst, the adsorption of HOO* should be thermoneutral at the equilibrium potential ($U^0_{O_2/H_2O_2}$ = 0.7 V),

Received: January 5, 2014
Revised: January 28, 2014

   dx.doi.org/10.1021/nl500037x | *Nano Lett.* XXXX, XXX, XXX−XXX

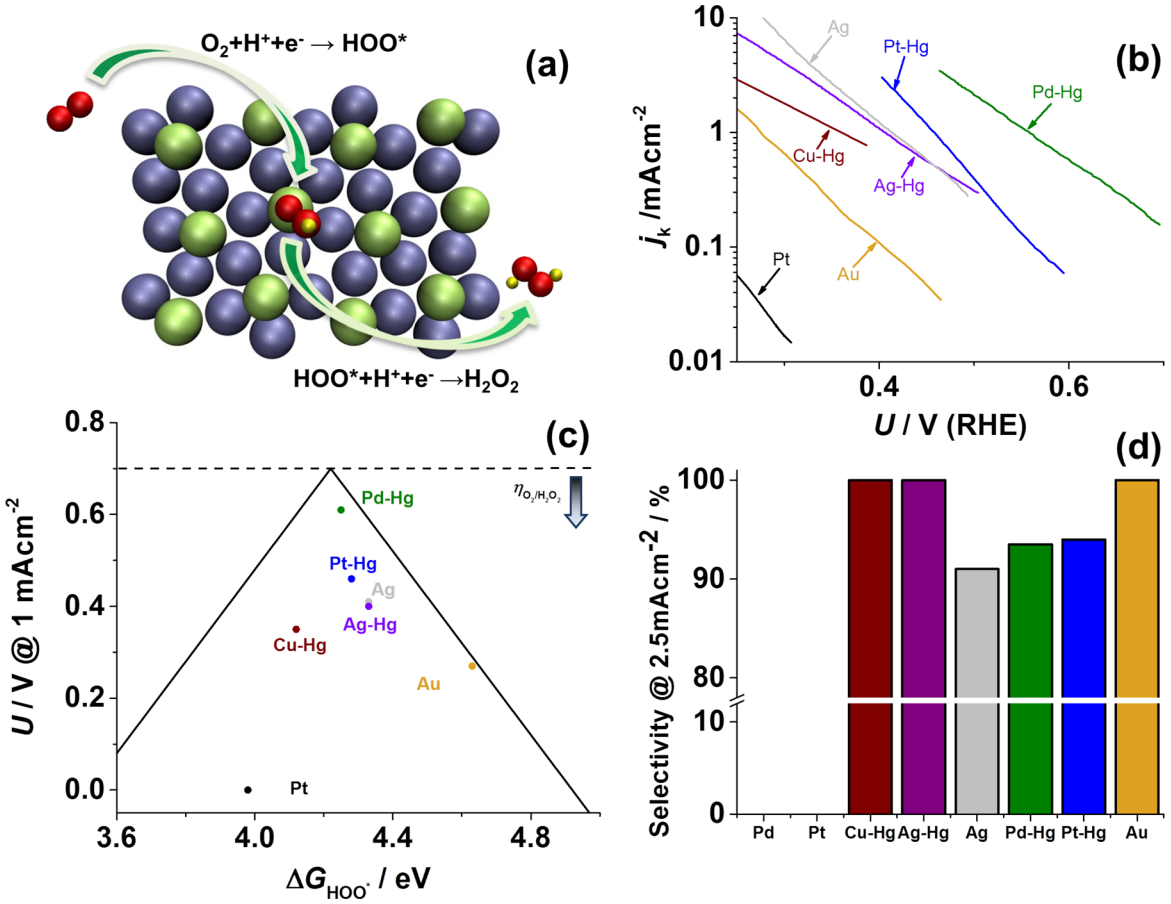

Figure 1. Trends in activity and selectivity for H_2O_2 production. (a) Schematic representation of oxygen reduction to H_2O_2 on a model Pd_2Hg_5 (001) surface. Palladium atoms are represented in green, mercury in blue, oxygen in red, and hydrogen in yellow. (b) Partial kinetic current density to H_2O_2 as a function of the applied potential, corrected for mass transport losses. (c) Potential required to reach 1 $mAcm^{-2}$ of kinetic current density to H_2O_2 on polycrystalline catalysts as a function of the calculated HOO* binding energy. The solid lines represent the theoretical Sabatier volcano.[21] The dotted line represents the thermodynamic potential for oxygen reduction to H_2O_2. (d) H_2O_2 selectivity for different catalysts at 2.5 $mAcm^{-2}$ of total current density. For this figure, data for Cu−Hg was extrapolated for ~100 mV as it is unstable above 0.25 V.[27] Data for Au adapted from Jirkovsky et al.,[28] data for Pt from Verdaguer-Casadevall et al.,[48] and data for Pt−Hg from Siahrostami et al.[20] All electrochemical experiments were performed at 50 mV s^{-1} and 1600 rpm in O_2-saturated 0.1 M $HClO_4$ at room temperature with corrections for Ohmic drop. The surface area was normalized to the geometrical value.

so that the theoretical overpotential for the reaction, $\eta = 0$. Stronger or weaker binding to HOO* will introduce additional overpotential, or lower electrocatalytic activity. This means that the theoretical overpotential should show a Sabatier-volcano type dependence on the HOO* adsorption energy, ΔG_{HOO}.

Selectivity is determined by the ability of the catalyst to split the O−O bond during the oxygen reduction reaction, preventing water formation ($U^0_{O_2/H_2O}$ = 1.23 V). The most successful catalysts in this respect include Co porphyrins[22] and Pd−Au.[7] They rely on the presence of isolated sites of a reactive atom, Co or Pd, surrounded by more inert atoms, N, C, and Au. Such sites are unable to break the O−O bond, ensuring a high selectivity to H_2O_2.

On the basis of the above ideas, we recently discovered a new catalyst for H_2O_2 production. Our density functional theory calculations identified Pt−Hg as a highly active and selective catalyst for the reaction. Our experiments confirmed the theoretical predictions, showing that both extended surfaces and nanoparticles of Pt−Hg are highly active and selective for oxygen reduction to H_2O_2.[20] In the current study, our goal is to systematically study trends for H_2O_2 production on both pure metals and alloy surfaces. We identify the most promising catalysts using well-characterized extended surfaces. Density functional theory (DFT) calculations are used to rationalize the observed trends. We then apply this knowledge gained from the model surfaces to produce the catalyst in a technologically relevant form, that is, nanoparticles. This approach serves as a general example of how improved catalysts can be developed via a fundamental understanding of the factors controlling their performance in an electrochemical environment.

When Hg is electrodeposited on Pt, the two metals form an ordered intermetallic at room temperature where isolated Pt atoms are surrounded by Hg.[23] The same electrodeposition procedure can be performed to modify other metals in particular Cu, Pd, and Ag. We choose these metals as they all alloy with Hg[24−26] and they exhibit at least some stability against dissolution under the acidic conditions and potential range where O_2 reduction to H_2O_2 would take place (i.e., 0 to 0.7 V).[27] Further details regarding the preparation and characterization of these extended surfaces can be found in the Supporting Information.

On Figure 1b, we plot the partial current densities to hydrogen peroxide production, corrected for mass transport, on polycrystalline electrodes as a function of the applied potential.

dx.doi.org/10.1021/nl500037x | Nano Lett. XXXX, XXX, XXX−XXX

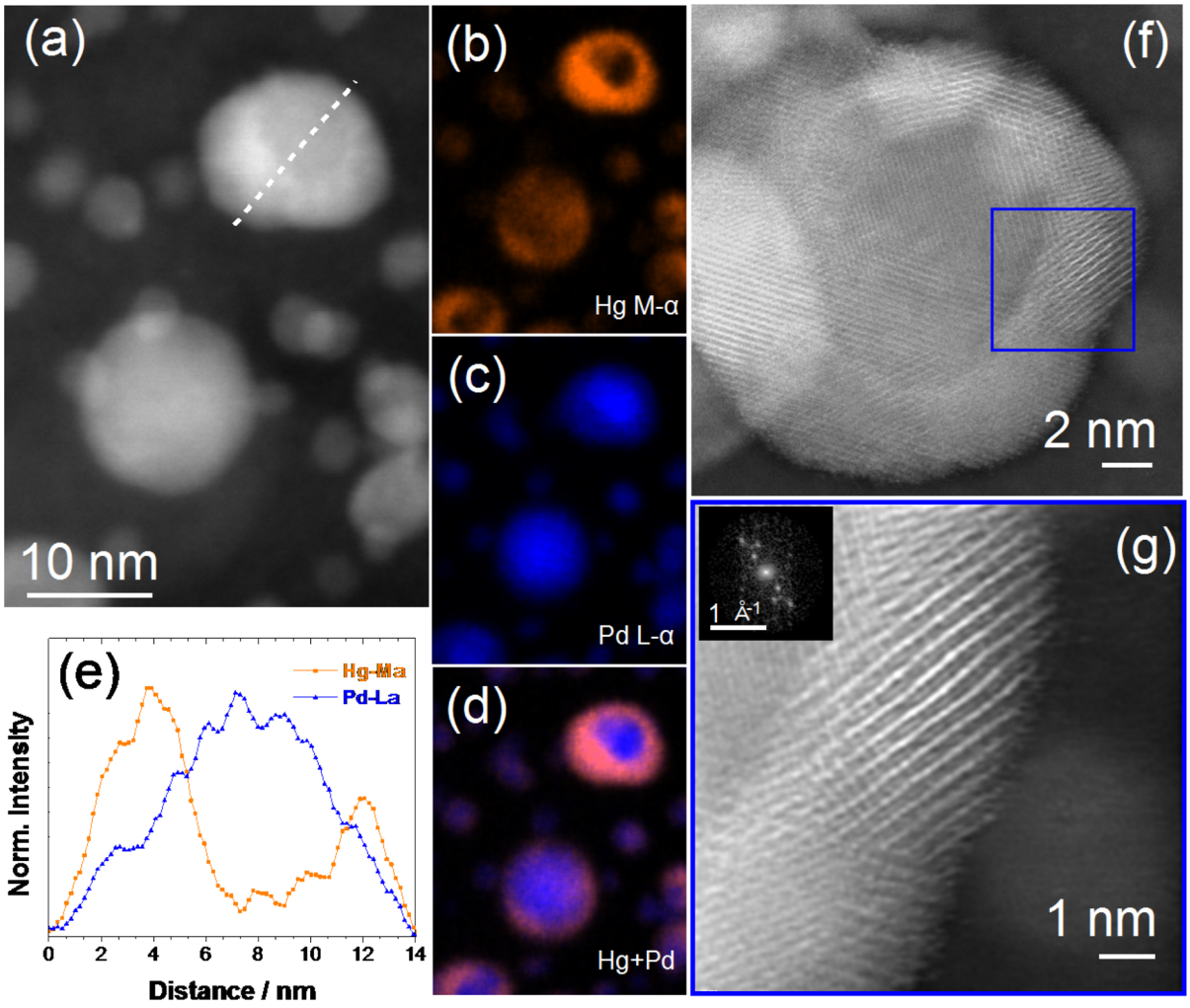

Figure 2. Electron microscopy characterization of Pd−Hg nanoparticles. (a) HAADF-STEM image of Pd−Hg nanoparticles and respective Hg, Pd, and Hg+Pd STEM-EDS elemental maps (b−d). (e) Normalized EDS Hg-Mα (orange) and Pd-Lα (blue) intensity line profiles extracted from the spectrum image data cube along with the white dashed line drawn on (a). (f) Fourier-filtered HAADF-STEM image of a Pd−Hg nanoparticle, showing a visible core−shell structure. (g) High-magnification HAADF-STEM image of the region enclosed in the blue square in (f); the inset shows the FFT of the bright fringes region.

Clearly, the electrode material has a decisive effect on the overpotential. In particular, the highest current at the lowest overpotential is obtained on Pd−Hg electrodes, while Pt−Hg, Ag−Hg, and Cu−Hg present increasing overpotentials. Notably, pure Ag has a high activity for this reaction, similar to that of Pt−Hg. All these materials are more active than Au-based catalysts, which have been extensively investigated in previous studies;[7,28,29] Pt−Hg, Ag, and Ag−Hg exhibit an order of magnitude improvement over Au, whereas the activity of Pd−Hg is 2 orders of magnitude higher.

To rationalize these findings, we used DFT to calculate ΔG_{HOO}* on the active sites for the reaction. Extensive details regarding the calculations are available in the Supporting Information. On Figure 1c, we plot the experimental overpotential required to reach 1 mAcm^{-2} of current to H_2O_2 for different catalysts, as a function of ΔG_{HOO}*. In particular, Pd−Hg exhibits the lowest overpotential, or highest activity, because it lies closest to the peak of the volcano. Catalysts such as Au or Ag bind HOO* too weakly, which means that their overpotential is due to the lack of formation of HOO* from O_2. All these catalysts lie on the right leg of the volcano and their activity follows the HOO* binding energy. On the other hand, the left leg of the volcano is somewhat steeper than the theoretical Sabatier volcano would suggest. The reason for this is selectivity: catalysts at the left leg will tend to favor water formation over H_2O_2.[20,21] Therefore, catalysts on the left leg will not typically produce any measurable amounts of H_2O_2. Nonetheless, H_2O_2 can be produced from such strong binding surfaces under conditions of accelerated mass transport.[30,31] Otherwise, should the catalysts on the left leg of the volcano lack the ensembles of atoms required to dissociate the O−O bond, they will also show some selectivity to H_2O_2; this is the case on pure Pt, below ∼0.3 V, where its surface is covered by adsorbed hydrogen,[19] or on Cu−Hg, where the Cu surface atoms are isolated from each other (see Supporting Information). Despite these limitations, the volcano captures the overall trends. Moreover, to the best of our knowledge this is the first time that these trends for H_2O_2 production are confirmed experimentally.

The selectivity to H_2O_2 is much higher on Hg-modified electrodes than on pure metal surfaces. In the case of Pd−Hg and Cu−Hg, we anticipate that the structure of the active site resembles that of Pt−Hg,[23] that is, single atoms of Pd or Cu, surrounded by Hg. At least two contiguous reactive atoms are

dx.doi.org/10.1021/nl500037x | Nano Lett. XXXX, XXX, XXX−XXX

required to dissociate HOO*, break the O−O bond and form the intermediates of the 4-electron reduction reaction, O* and HO*.[7,32] Consequently, monatomic sites are unable to break the O−O bond, making them selective for H_2O_2 production.

In the case of Ag−Hg, the cause of its high selectivity at 100% over the entire potential range is subtly different. The alloy has only a slightly negative enthalpy of formation at −0.03 eV/atom[26] as described in the Supporting Information. For this reason, the compound forms a solid solution, rather than an ordered intermetallic. Within such a solid solution, there will be regions close to pure Ag and other regions close to pure Hg; this would explain why the activity is equal or slightly lower to that of pure Ag. We hypothesize that the reason for the very high selectivity of Ag−Hg is due to the preferential deposition of Hg on the steps of Ag.[33] DFT calculations show that the barrier for HOO* (or H_2O_2) dissociation is much higher on terrace sites than on step sites.[34] This means that steps should be inherently more selective toward the 4-electron reduction than terraces. Blocking them with Hg provides a means of ensuring high selectivity to H_2O_2 production.

The industrial implementation of electrochemical H_2O_2 production requires well dispersed catalysts with a high current density per unit mass in order to be economically competitive.[35,36] On the basis of the results obtained for extended surfaces, Pd−Hg has an intrinsically higher activity than any other catalyst reported thus far. Below, we translate this improvement into technologically relevant Pd−Hg/C nanoparticles.

Pd/C was prepared in an ink and drop cast on a glassy carbon electrode, using the thin film rotating disk electrode technique.[37] The oxygen reduction activity was measured on the pure Pd catalyst and found to agree closely with literature values,[38] validating our experimental procedure (see Supporting Information). Following this, we electrodeposited mercury onto the electrode.

The catalyst composition was verified by scanning transmission electron microscopy (STEM) and X-ray energy dispersive spectroscopy (EDS). Figure 2f shows the high-angle annular dark-field (HAADF)-STEM image of a Pd−Hg nanoparticle. A difference in contrast between the central and outer regions of the particle is clearly visible. The HAADF signal intensity has a strong dependence with the atomic number, hence the brighter regions around the central zone of the nanoparticle indicate an Hg-rich thick surface, suggesting a core−shell structure. A closer inspection of the shell region shown in Figure 2g reveals alternating high contrast lattice fringes with spacing of 2.9 ± 0.2 Å. This is consistent with the 3.0310 Å distance separating the (001) planes of the Pd_2Hg_5 alloy structure.[25] Furthermore, these planes contain only Hg atoms and consequently appear brighter in the HAADF image. In order to confirm the presence of the Hg-rich shell, STEM-EDS mapping was performed. The STEM image and the corresponding EDS elemental maps of a region with different nanoparticles are shown in Figure 2a−d. The combined Hg and Pd elemental maps unmistakably show that a core−shell structure is formed with an anisotropic thickness of the shell. This can be visualized even more clearly by the EDS intensity profile linescan in Figure 2e. The anisotropy in the shell thickness can be ascribed to the different reactivity of each facet on the nanoparticle. The alloying of Pd and Hg was also confirmed by X-ray photoelectron spectroscopy (see Supporting Information). Further proof of the structure is shown in the Supporting Information. Taken as a whole, the TEM images in Figure 2 demonstrate that the nanoparticles form a core−shell structure at room temperature. The core is Pd, whereas the shell consists of an ordered intermetallic, likely Pd_2Hg_5. This is the same structure that was modeled in our DFT calculations, whose (001) facet we used to simulate the highly active and selective extended polycrystalline Pd−Hg surfaces described above.

Oxygen reduction on Pd−Hg/C nanoparticles shows a very similar behavior to polycrystalline Pd−Hg (Figure 3d). Upon saturation of the electrolyte with O_2, we observed a negative current corresponding to oxygen reduction. The ring current shows that a substantial amount of the disk current is due to

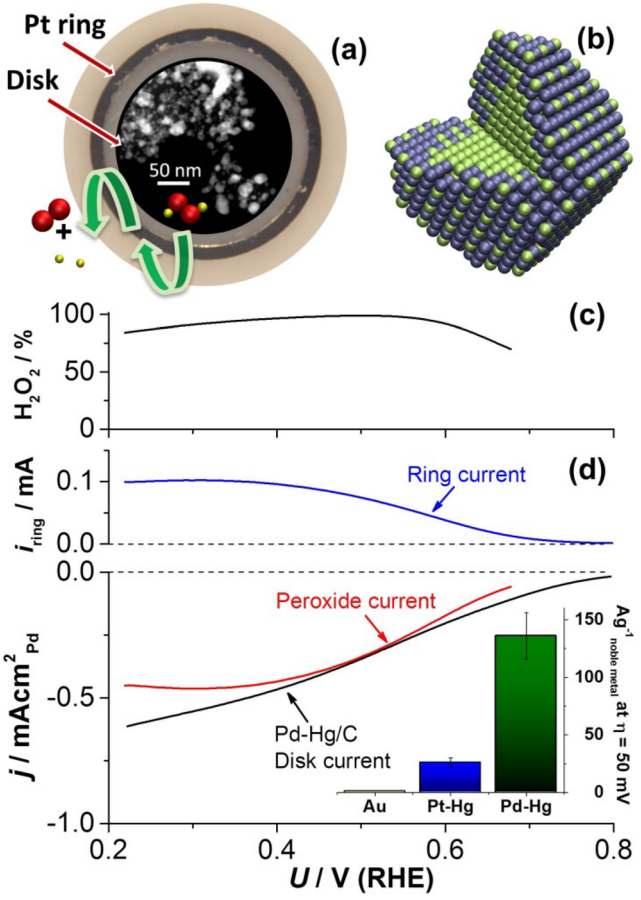

Figure 3. Electrochemical characterization of Pd−Hg/C nanoparticles. (a) Rotating ring-disk electrode with a schematic representation of H_2O_2 oxidation at the ring. The disk has been modified to show a HAADF-STEM overview of the Pd−Hg/C nanoparticles. (b) Schematic representation of a Pd−Hg nanoparticle with Pd colored in green and Hg in blue. (c) H_2O_2 selectivity as a function of the applied potential. (d) RRDE voltammograms at 1600 rpm in O_2-saturated electrolyte with the disk current (black), ring current (blue) and corresponding current to hydrogen peroxide (red) obtained from the ring current (only the anodic cycle is shown). The disk current is normalized to the surface area of Pd nanoparticles (estimated from the oxide reduction peak before deposition of Hg). The inset shows the mass activity (A per g of noble metal) at 50 mV of overpotential for nanoparticulate catalysts. Data for Pt−Hg adapted from Siahrostami et al.[20] All electrochemical experiments were performed at 50 mV s^{-1} and 1600 rpm in O_2 saturated 0.1 M $HClO_4$ at room temperature with corrections for Ohmic drop and capacitive currents.[49] Full details on the normalization procedure and mass activity calculations are available in the Supporting Information.

dx.doi.org/10.1021/nl500037x | Nano Lett. XXXX, XXX, XXX−XXX

hydrogen peroxide production with a selectivity higher than 95% between 0.35 and 0.55 V (Figure 3c). At 50 mV overpotential, Pd−Hg/C presents an activity per mass of precious metal five times higher than Pt−Hg/C and more than 2 orders of magnitude higher than state-of-the-art Au/C (inset of Figure 3d). In addition, Pd−Hg/C is highly stable, displaying negligible losses after 8000 potential cycles between 0.2 and 0.7 V.

In summary, we have modified different metal surfaces with Hg, as a means to tune the oxygen reduction activity and selectivity of various electrodes toward H_2O_2 production. By using a combination of theory and experiments, we have verified that the activity can be described by the *HOO binding energy, via a Sabatier-volcano. Selectivity in turn is described by the geometric arrangement of the catalyst sites. This approach led to the discovery of both Ag−Hg and Pd−Hg as catalysts for H_2O_2 production. The deployment of either catalyst could bring about significant improvements to the efficiency, selectivity, and cost[39] of a H_2O_2 producing device, in comparison to the current state-of-the art.[7,20] Fine tuning the particle shape, size, and composition should lead to an even higher activity per mass of precious metal.[40−44] Nonetheless, future progress will be grounded on the basis of the active sites developed in this work. The concepts used here to tune oxygen reduction activity and selectivity can be extended to other reactions such as the reduction of CO_2[45,46] or the selective oxidation of hydrocarbons.[47]

■ ASSOCIATED CONTENT

Ⓢ Supporting Information

Detailed description of experimental and theoretical methods, as well as additional voltammetric data, characterization results, and DFT calculations. This material is available free of charge via the Internet at http://pubs.acs.org.

■ AUTHOR INFORMATION

Corresponding Authors

*E-mail: (I.C.) ibchork@fysik.dtu.dk.
*E-mail: (I.E.L.S.) ifan@fysik.dtu.dk.

Author Contributions

A.V. and I.E.L.S. developed the idea and designed the experiments. A.V. performed the electrochemical experiments, D.D. performed the microscopy, and P.M. performed the XPS. M.K. and S.S. performed the theoretical calculations. A.V. and I.E.LS. wrote the first draft of the paper. A.V. and D.D. designed the figures. All authors discussed the results and commented on the manuscript.

Notes

The authors declare the following competing financial interest(s): Some of the authors of this manuscript were inventors on patent application EP 13165265.3 Alloy catalyst material. This patent includes some of the catalyst materials described here within its scope..

■ ACKNOWLEDGMENTS

The authors gratefully acknowledge financial support from the Danish Ministry of Science's UNIK initiative, Catalysis for Sustainable Energy. The Danish National Research Foundation's Center for Individual Nanoparticle Functionality is supported by the Danish National Research Foundation (DNRF54). The A.P. Møller and Chastine Mc-Kinney Møller Foundation is gratefully acknowledged for its contribution towards the establishment of the Centre for Electron Nanoscopy in the Technical University of Denmark. The Interdisciplinary Centre for Electron Microscopy (CIME) at EPFL is gratefully acknowledged for the use of the FEI Tecnai Osiris TEM.

■ REFERENCES

(1) Chorkendorff, I.; Niemantsverdriet, J. W. *Concepts of Modern Catalysis and Kinetics*, student ed.; Wiley-VCH Verlag GmbH & Co. KGaA: Weinheim, 2003.
(2) Kotrel, S., Brauninger, S. *Handbook of Heterogeneous Catalysis*, 2nd ed.; Ertl, G., Knoezinger, H., Schueth, F., Weitkamp, J., Eds.; Wiley: New York, 2008.
(3) Campos-Martin, J. M.; Blanco-Brieva, G.; Fierro, J. L. G. *Angew. Chem., Int. Ed.* **2006**, *45* (42), 6962−6984.
(4) *Ullman's Encyclopedia of Industrial Chemistry*; Wiley: New York, 1999−2013.
(5) Edwards, J. K.; Solsona, B.; N, E. N.; Carley, A. F.; Herzing, A. A.; Kiely, C. J.; Hutchings, G. J. *Science* **2009**, *323* (5917), 1037−1041.
(6) Samanta, C. *Appl. Catal., A* **2008**, *350* (2), 133−149.
(7) Jirkovský, J. S.; Panas, I.; Ahlberg, E.; Halasa, M.; Romani, S.; Schiffrin, D. J. *J. Am. Chem. Soc.* **2011**, *133* (48), 19432−19441.
(8) Fellinger, T.-P.; Hasché, F.; Strasser, P.; Antonietti, M. *J. Am. Chem. Soc.* **2012**, *134* (9), 4072−4075.
(9) Yamanaka, I.; Onizawa, T.; Takenaka, S.; Otsuka, K. *Angew. Chem.* **2003**, *115* (31), 3781−3783.
(10) Parsons, R. *Trans. Faraday Soc.* **1958**, *54* (7), 1053−1063.
(11) Trasatti, S. *J. Electroanal. Chem.* **1972**, *39* (1), 163−&.
(12) Stamenkovic, V. R.; Mun, B. S.; Arenz, M.; Mayrhofer, K. J. J.; Lucas, C. A.; Wang, G.; Ross, P. N.; Markovic, N. M. *Nat. Mater.* **2007**, *6* (3), 241−247.
(13) Greeley, J.; Stephens, I. E. L.; Bondarenko, A. S.; Johansson, T. P.; Hansen, H. A.; Jaramillo, T. F.; Rossmeisl, J.; Chorkendorff, I.; Nørskov, J. K. *Nature Chem.* **2009**, *1* (7), 552−556.
(14) Suntivich, J.; May, K. J.; Gasteiger, H. A.; Goodenough, J. B.; Shao-Horn, Y. *Science* **2011**, *334* (6061), 1383−1385.
(15) Stephens, I. E. L.; Bondarenko, A. S.; Perez-Alonso, F. J.; Calle-Vallejo, F.; Bech, L.; Johansson, T. P.; Jepsen, A. K.; Frydendal, R.; Knudsen, B. P.; Rossmeisl, J.; Chorkendorff, I. *J. Am. Chem. Soc.* **2011**, *133* (14), 5485−5491.
(16) Subbaraman, R.; Tripkovic, D.; Chang, K.-C.; Strmcnik, D.; Paulikas, A. P.; Hirunsit, P.; Chan, M.; Greeley, J.; Stamenkovic, V.; Markovic, N. M. *Nat. Mater.* **2012**, *11* (6), 550−557.
(17) Bandarenka, A. S.; Varela, A. S.; Karamad, M.; Calle-Vallejo, F.; Bech, L.; Perez-Alonso, F. J.; Rossmeisl, J.; Stephens, I. E. L.; Chorkendorff, I. *Angew. Chem., Int. Ed.* **2012**, *51* (47), 11845−11848.
(18) Hinnemann, B.; Moses, P. G.; Bonde, J.; Jorgensen, K. P.; Nielsen, J. H.; Horch, S.; Chorkendorff, I.; Nørskov, J. K. *J. Am. Chem. Soc.* **2005**, *127* (15), 5308−5309.
(19) Stamenkovic, V. R.; Fowler, B.; Mun, B. S.; Wang, G.; Ross, P. N.; Lucas, C. A.; Marković, N. M. *Science* **2007**, *315* (5811), 493−497.
(20) Siahrostami, S.; Verdaguer-Casadevall, A.; Karamad, M.; Deiana, D.; Malacrida, P.; Wickman, B.; Escudero-Escribano, M.; Paoli, E. A.; Frydendal, R.; Hansen, T. W.; Chorkendorff, I.; Stephens, I. E. L.; Rossmeisl, J. *Nat. Mater.* **2013**, *12* (12), 1137−1143.
(21) Viswanathan, V.; Hansen, H. A.; Rossmeisl, J.; Nørskov, J. K. *J. Phys. Chem. Lett.* **2012**, *3* (20), 2948−2951.
(22) Jaouen, F.; Proietti, E.; Lefevre, M.; Chenitz, R.; Dodelet, J.-P.; Wu, G.; Chung, H. T.; Johnston, C. M.; Zelenay, P. *Energy Environ. Sci.* **2011**, *4* (1), 114−130.
(23) Wu, H. L.; Yau, S.; Zei, M. S. *Electrochim. Acta* **2008**, *53* (20), 5961−5967.
(24) Russell, A. S.; Kennedy, T. R.; Howitt, J.; Lyons, H. A. M. *J. Chem. Soc.* **1932**, 2340−2342.
(25) Guminski, C. *Bull. Alloy Phase Diagrams* **1990**, *11* (1), 22−26.
(26) Baren, M. R. *J. Phase Equilib.* **1996**, *17* (2), 122−128.
(27) Pourbaix, M. *Atlas of electrochemical equilibria in aqueous solutions, National Association of Corrosion Engineers*, **1974**.

(28) Jirkovsky, J. S.; Halasa, M.; Schiffrin, D. J. *Phys. Chem. Chem. Phys.* **2010**, *12* (28), 8042−8053.
(29) Erikson, H.; Jürmann, G.; Sarapuu, A.; Potter, R. J.; Tammeveski, K. *Electrochim. Acta* **2009**, *54* (28), 7483−7489.
(30) Chen, S.; Kucernak, A. *J. Phys. Chem. B* **2004**, *108* (10), 3262−3276.
(31) Schneider, A.; Colmenares, L.; Seidel, Y. E.; Jusys, Z.; Wickman, B.; Kasemo, B.; Behm, R. J. *Phys. Chem. Chem. Phys.* **2008**, *10* (14), 1931−1943.
(32) Siahrostami, S.; Bjorketun, M. E.; Strasser, P.; Greeley, J.; Rossmeisl, J. *Phys. Chem. Chem. Phys.* **2013**, *15* (23), 9326−9334.
(33) Levlin, M.; Ikävalko, E.; Laitinen, T. *Fresenius J. Anal. Chem.* **1999**, *365* (7), 577−586.
(34) Rankin, R. B.; Greeley, J. *ACS Catal.* **2012**, *2* (12), 2664−2672.
(35) Stephens, I. E. L.; Bondarenko, A. S.; Gronbjerg, U.; Rossmeisl, J.; Chorkendorff, I. *Energy Environ. Sci.* **2012**.
(36) Gasteiger, H. A.; Markovic, N. M. *Science* **2009**, *324* (5923), 48−49.
(37) Schmidt, T. J.; Gasteiger, H. A.; Stab, G. D.; Urban, P. M.; Kolb, D. M.; Behm, R. J. *J. Electrochem. Soc.* **1998**, *145* (7), 2354−2358.
(38) Shao, M.-H.; Sasaki, K.; Adzic, R. R. *J. Am. Chem. Soc.* **2006**, *128* (11), 3526−3527.
(39) Vesborg, P. C. K.; Jaramillo, T. F. *RSC Adv.* **2012**, *2* (21), 7933−7947.
(40) Sasaki, K.; Naohara, H.; Cai, Y.; Choi, Y. M.; Liu, P.; Vukmirovic, M. B.; Wang, J. X.; Adzic, R. R. *Angew. Chem., Int. Ed.* **2010**, *49* (46), 8602−8607.
(41) Guo, S.; Li, D.; Zhu, H.; Zhang, S.; Markovic, N. M.; Stamenkovic, V. R.; Sun, S. *Angew. Chem., Int. Ed.* **2013**, *52* (12), 3465−3468.
(42) Cui, C.; Gan, L.; Heggen, M.; Rudi, S.; Strasser, P. *Nat. Mater.* **2013**, *12* (8), 765−771.
(43) Mayrhofer, K. J. J.; Juhart, V.; Hartl, K.; Hanzlik, M.; Arenz, M. *Angew. Chem., Int. Ed.* **2009**, *48* (19), 3529−3531.
(44) Wang, D. L.; Xin, H. L. L.; Hovden, R.; Wang, H. S.; Yu, Y. C.; Muller, D. A.; DiSalvo, F. J.; Abruna, H. D. *Nat. Mater.* **2013**, *12* (1), 81−87.
(45) Kuhl, K. P.; Cave, E. R.; Abram, D. N.; Jaramillo, T. F. *Energy Environ. Sci.* **2012**, *5* (5), 7050−7059.
(46) Li, C. W.; Kanan, M. W. *J. Am. Chem. Soc.* **2012**, *134* (17), 7231−7234.
(47) Tomita, A.; Nakajima, J.; Hibino, T. *Angew. Chem., Int. Ed.* **2008**, *47* (8), 1462−1464.
(48) Verdaguer-Casadevall, A.; Hernandez-Fernandez, P.; Stephens, I. E. L.; Chorkendorff, I.; Dahl, S. *J. Power Sources* **2012**, *220* (0), 205−210.
(49) Nesselberger, M.; Ashton, S.; Meier, J. C.; Katsounaros, I.; Mayrhofer, K. J. J.; Arenz, M. *J. Am. Chem. Soc.* **2011**, *133* (43), 17428−17433.

dx.doi.org/10.1021/nl500037x | *Nano Lett.* XXXX, XXX, XXX−XXX